Anelastic internal friction of dislocations in two-dimensional Yukawa solids

Shaoyu Lu,[1] Dong Huang,[1] Chen Liang,[1] and Yan Feng[1,2,*]

[1]*Institute of Plasma Physics and Technology, Jiangsu Key Laboratory of Thin Films, School of Physical Science and Technology, Soochow University, Suzhou 215006, China*

[2]*National Laboratory of Solid State Microstructures, Nanjing University, Nanjing 210093, China*

(Received 6 September 2023; accepted 10 October 2023; published 3 November 2023)

Langevin dynamical simulations are performed to investigate the dislocation internal friction (IF) of solid two-dimensional (2D) dusty plasmas under oscillating shear deformations. The magnitude of IF is quantified using the loss factor Q^{-1} from the stress-strain hysteresis. It is discovered that the dislocation IF is significantly dependent on the dislocation's slip direction relative to the shear direction. It is found that the variation trend of the dislocation IF with the dislocation's slip direction is positively related to the dislocation's slip distance, while the energy loss occurs due to the generation of shear bands. The dislocation IF in solid 2D dusty plasmas is found to be heavily dependent on the shear deformation frequency, while nearly independent of the shear strain amplitude, corresponding to a typical anelastic property.

DOI: 10.1103/PhysRevResearch.5.043116

I. INTRODUCTION

Internal friction (IF) is generally defined as the mechanical energy dissipation inside a material [1–4]. In a solid material, IF usually refers to the energy dissipation related to the deviation from Hooke's law, which is manifested from the stress-strain hysteresis under the cyclic loading [4]. Also known as mechanical spectroscopy, IF measurements are widely performed in solid state physics, physical metallurgy, and various engineering applications [2–10]. To quantify the magnitude of the IF, the loss factor is mostly used, which can be defined as [1–4]

$$Q^{-1} = \Delta W/2\pi W. \tag{1}$$

Here, ΔW is the corresponding dissipated energy during one deformation cycle, while W is the maximum elastic stored energy during that cycle.

The definition of anelasticity was first proposed in 1948 [1] to separate it from the more general viscoelastic behavior. Under external loading, the deformed solid may undergo a series of transitions from elastic to anelastic and then microplastic or even, finally, plastic [3]. The transition from elastic to plastic is characterized by irreversible macroscopic deformation. However, the anelastic transition is caused by structural defects in solids within the elastic deformation range, which are the sources of the mechanical energy scattering. Anelasticity meets the requirements of the law of elasticity, such as each stress value corresponding to only one equilibrium value of the strain and vice versa, as well as the linear stress-strain response [11]. As compared with the traditional elastic behavior, the anelastic behavior exhibits a noninstantaneous stress-strain response, so that a relaxation process is needed to achieve the linear stress-strain response [11]. For the anelastic behavior [3,4,11], the elastic modulus can be separated into two parts, namely, the energy storage and dissipation portions, which are strongly related to the frequency and independent from the stress level or the strain amplitude. The IF caused by this relaxation process is called the anelastic IF.

Dusty plasma, or complex plasma, typically refers to a collection of micrometer-sized dust particles in the plasma environment [12–25]. Under typical laboratory conditions, dust particles are highly charged to approximately $-10^4 e$, so that tens of thousands of these dust particles can form a single-layer suspension in the plasma sheath, i.e., the two-dimensional (2D) dusty plasma [26–28]. Since these dust particles are highly charged, the potential energy between neighboring dust particles is much higher than their kinetic energy, i.e., these dust particles are strongly coupled, exhibiting the collective properties of liquids [22,29–33] or solids [34–40]. Due to the individual particle identification and tracking in experiments, dusty plasma provides an excellent platform to study various behaviors of solids at the individual particle level, such as elastic [41–47], viscoelastic [33,48], and plastic [38,39,49] behaviors. However, in our literature search, we have not found any previous investigations of the anelastic behavior or IF in dusty plasmas, which we will study here.

This paper is organized as follows. In Sec. II, we introduce our simulation method to mimic solid 2D dusty plasmas under uniform oscillating shear deformations. In Sec. III, we calculate the dislocation IF of our simulated solid 2D dusty plasma for various dislocation slip directions, different shear strain amplitudes, and varying shear deformation frequencies. Furthermore, to study the underlying mechanism of the dislocation IF, we also calculate the distributions of the average

*fengyan@suda.edu.cn

atomic shear strain and atomic elastic constant. Finally, we provide a brief summary in Sec. IV.

II. SIMULATIONS

To mimic solid 2D dusty plasmas under uniform oscillating shear deformations, we perform Langevin dynamical simulations of 2D Yukawa solids with $N = 4096$ dust particles using Large-Scale Atomic/Molecular Massively Parallel Simulator (LAMMPS) [50]. For each particle i, the equation of motion within a 2D plane is

$$m\ddot{\mathbf{r}}_i = -\nabla\Sigma\phi_{ij} - \nu m\dot{\mathbf{r}}_i + \zeta_i(t), \tag{2}$$

where the three terms on the right-hand side are the interparticle Yukawa repulsion $\phi_{rj} = Q^2\exp(-r_{rj}/\lambda_D)/4\pi\epsilon_0 r_{rj}$, the frictional gas drag [51], and the Langevin random kicks [52], respectively. Here, r_{ij} is the distance between particles i and j, Q is the particle charge, and λ_D is the screening length.

Following the tradition of Refs. [17,43,44], we use the coupling parameter Γ and the screening parameter κ to characterize 2D dusty plasmas. These two parameters are defined as $\Gamma = Q^2/(4\pi\epsilon_0 a k_B T)$ and $\kappa = a/\lambda_D$, respectively, where T is the kinetic temperature of dust particles, k_B is the Boltzmann constant, and a is the Wigner-Seitz radius $(1/n\pi)^{1/2}$ for the 2D areal number density of n [17]. To normalize the time scale, we use the nominal 2D dusty plasma frequency [17] $\omega_{pd} = \sqrt{Q^2/2\pi\epsilon_0 m a^3}$. In this paper, we keep the unchanged values of $\kappa = 0.5$ and $\Gamma = 800$, corresponding to a typical solid state for 2D dusty plasmas [53]. Note that our simulated $N = 4096$ dust particles are all confined in a 2D plane of $L_x \times L_y$, where $L_x = 121.896a$ and $L_y = 105.565a$.

The uniform oscillating shear deformation is applied in the x direction using the Lees-Edwards periodic boundary conditions [54]. The shear strain is specified as a sinusoidal function of

$$\gamma(t) = \gamma_0 \sin(\omega t). \tag{3}$$

Here, ω is the shear deformation frequency, while the shear strain amplitude γ_0 is a dimensionless measure of deformation, defined as the ratio of the length change along the shear direction to the reference length perpendicular to the shear, i.e., $\Delta x/L_y$. We vary the shear strain amplitude γ_0 from 0.019 to 0.057; these values are much smaller than the elastic upper limit of the softer 2D Yukawa crystal of $\kappa = 0.75$ [42,47]. Furthermore, from the strain-stress response tests performed here in the corresponding perfect crystal of $\kappa = 0.5$ and $\Gamma = 800$, we also confirm that our specified shear strain amplitude is always in the apparent linear elastic regime. The shear deformation frequency ω/ω_{pd} is varied from 0.0001 to 0.005; these frequencies are much slower than the motion of individual particles. With the specified values of γ_0 and ω above, the applied oscillating shear deformation of our simulated solid 2D dusty plasma can be approximately regarded as a series of quasistatic processes.

To prepare suitable initial configurations for our anelastic IF investigation, each simulation run always starts from a fully annealed solid lattice under the conditions of $\kappa = 0.5$ and $\Gamma = 800$. After a full relaxation over a long time, there are usually only a few dislocations left in the final lattice. We only choose a lattice with just one pair of dislocations left, while others with more than two dislocations are abandoned. The lattice with only one pair of dislocations left is regarded as the initial configuration of our studied solid dusty plasma with defects. Next, we apply the oscillating shear strain of Eq. (1) to the initial configuration and then record the positions and velocities of all particles for at least ten cycles for the data analysis reported here. The integration time step is specified as either $1.41 \times 10^{-2}\omega_{pd}^{-1}$ or $7.07 \times 10^{-3}\omega_{pd}^{-1}$ for the lower or higher shear deformation frequencies. Note that the gas damping rate is specified as $\nu = 0.027\omega_{pd}$, comparable to typical experimental values [31,33]. Other simulation details are the same as in Ref. [47]. Here, we would like to clarify that we only focus on the IF caused by one pair of dislocations, so that the IF of high-temperature 2D Yukawa solids with more dislocations is well beyond the scope of this paper.

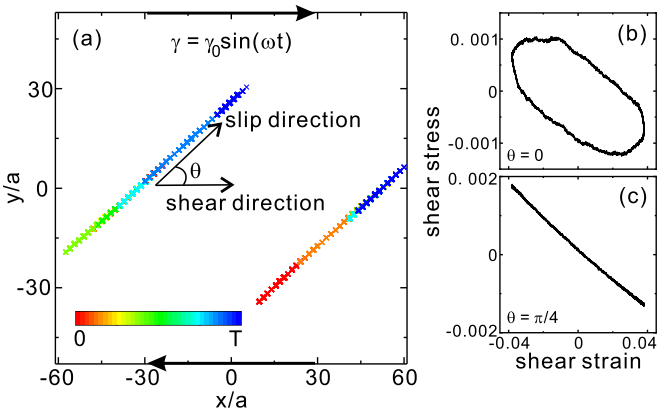

FIG. 1. Typical trajectories of dislocations in 2D Yukawa solids during one period of the oscillating shear deformation (a), as well as the obtained stress-strain responses under different conditions [(b) and (c)]. Under the oscillating shear deformation, dislocations mostly slip along one specific direction, as θ relative to the shear direction in (a). From (b), while dislocations slip along the direction of $\theta = 0$, the stress-strain curve exhibits a hysteresis, indicating the dissipation of the internal friction (IF). However, from (c), when the dislocations slip along $\theta = \pi/4$, the linear relationship between stress and strain without hysteresis clearly indicates that the energy dissipation is nearly zero.

III. RESULTS

A. IF dependence on dislocation slip direction

Figure 1(a) shows typical trajectories of a pair of dislocations within one shear deformation cycle. Due to the applied shear deformation, dislocations in 2D Yukawa solids slip along one specific direction with a constant angle θ relative to the shear direction, as shown in Fig. 1(a). For nearly all simulation runs of our current IF investigation with only one pair of dislocations inside the studied solid 2D dusty plasma, we confirm that the dislocation's slip direction does not change at all; that is, the dislocation's slip angle θ is only determined by the particle arrangement and the dislocation's location in the initial configuration. Only when the two dislocations collide with each other, or are extremely close to each other, would their slip angle change substantially. In fact, since the Burgers vectors of these two dislocations are reversely in parallel,

the two dislocations always slip in two completely opposite directions. Note that for the studied conditions with only one pair of dislocations, the dislocation is only able to slip along the principal axis of the lattice, so that the dislocations' slip angle can be regarded as the angle of the lattice orientation relative to the shear direction, as confirmed in our simulation data.

To quantify the magnitude of IF, we need to determine the dissipated energy per unit area ΔW and the maximum elastic energy per unit area W in Eq. (1). We calculate W using $W = G\gamma_0^2/2$ [11], where G is the shear modulus of 2D Yukawa solids derived from the theoretical transverse sound speed of a 2D Yukawa crystal C_T in the theory of Ref. [55] and the number density n using $G = mnC_T^2$ [42]. For our simulation condition of $\kappa = 0.5$, the obtained values of C_T and G are $0.25a\omega_{pd}$ and $0.040\sigma_0$, respectively. The dissipated energy per unit area ΔW is directly determined from the area of the enclosed region in the stress-strain response hysteresis [3,4]. After the external shear strain γ is applied, the time series of the shear stress P_{xy} is calculated as in Ref. [47]. Thus the stress-strain response relationship is obtained; two examples are shown in Figs. 1(b) and 1(c). Note that to easily compare our results with results for other systems, we normalize the obtained shear stress using $\sigma_0 = Q^2/4\pi\epsilon_0 a^3$, as in Ref. [47].

For our studied solid 2D dusty plasma undergoing applied periodic shear deformation, we find that the stress-strain response significantly varies with the dislocation's slip direction, as shown in Figs. 1(b) and 1(c). Clearly, when the dislocations slip along the direction of $\theta = 0$ [Fig. 1(b)], the stress-strain response exhibits a typical hysteresis, clearly indicating the significant energy dissipation. However, as seen in Fig. 1(c), when the dislocations slip along $\theta = \pi/4$, the response curve changes to a straight line instead, indicating that the dissipated energy is nearly zero.

As the major result of this paper, we discover the variation trend of the dislocation IF as a function of the dislocation's slip angle θ, presented in Fig. 2. We find that when the absolute value of θ varies from 0 to $\pi/4$, the value of Q^{-1} decreases from its maximum to zero monotonically. When $|\theta|$ increases from $\pi/4$ to $\pi/2$, the value of Q^{-1} increases from zero monotonically back to its maximum again. Note that for the data points presented in Fig. 2, the shear deformation frequency and the shear strain amplitude are specified as constant values of $\omega/\omega_{pd} = 0.001$ and $\gamma_0 = 0.038$, respectively. The error bars are determined by the standard deviation of the obtained Q^{-1} values from multiple deformation periods in the same simulation run. Note that besides the simulation results reported here, we also perform test runs with 16 384 particles, with the other conditions being the same, and we confirm that the IF variation trend under these conditions does not change from the trend in Fig. 2, although the IF value due to one pair of dislocations decreases due to the lower dislocation density.

The variation trend of Q^{-1} in Fig. 2 clearly indicates that the slip angle θ of dislocations has a significant effect on the magnitude of IF. Apparently, the IF is caused by the phase difference between the stress and the strain of the material. In essence, the IF occurs due to the existence of energy dissipation sources, which are structural defects inside the solid, as well as the motion and interaction of these defects in our studied system. Our observed variation trend Q^{-1} here is quite

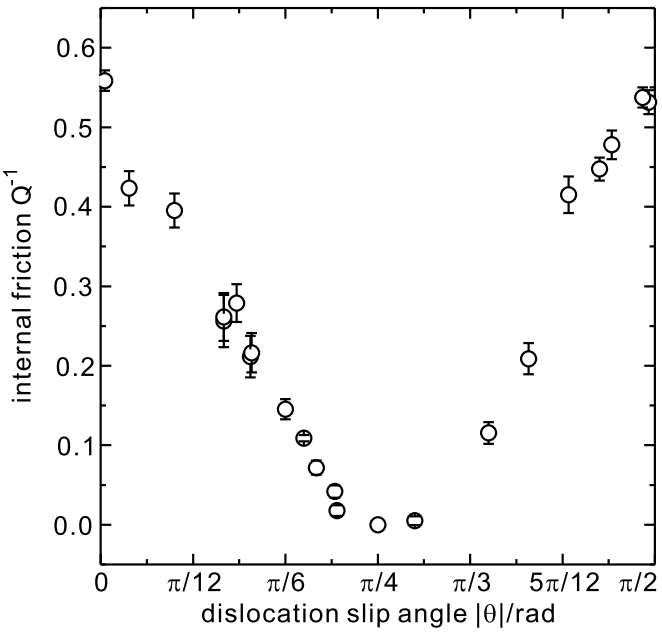

FIG. 2. Obtained dislocation IF Q^{-1} of 2D Yukawa solids as the slip angle of dislocations $|\theta|$ varies. When the slip angle θ increases gradually from 0 to $\pi/2$, the value of Q^{-1} first decreases to nearly zero when $|\theta| = \pi/4$ and then increases back nearly symmetrically. Note that for these results, the shear deformation frequency and the shear strain amplitude are specified as $\omega/\omega_{pd} = 0.001$ and $\gamma_0 = 0.038$, respectively.

similar to the IF results in real crystals [56,57], where the dislocation IF varies with the angle between the sample axis and the direction of the distribution of the ultrasound wave. Since the dissipation source of IF is only one pair of dislocations in our simulation, let us investigate the mechanism of the dislocation IF from the trajectories of dislocations in detail next.

B. IF due to dislocation slip motion

To explore the underlying mechanism of the dislocation IF in 2D Yukawa solids, we investigate the local strain caused by the slip motion of dislocations at the individual particle level. We quantify the atomic shear strain using

$$\widetilde{\gamma_{\rm vM}(i)} = \overline{\gamma_{\rm vM}(i)} - \langle\overline{\gamma_{\rm vM}(i)}\rangle, \tag{4}$$

where $\gamma_{\rm vM}(i)$ is the von Mises local shear invariant of the strain tensor [58] for particle i. Here, the overline refers to the mean of the corresponding quantity within one shear deformation period, while $\langle\ \rangle$ means the average over all particles within the whole simulation region. The von Mises local shear invariant [58] is a sensitive quantity to accurately measure the local shear deformation along any arbitrary directions, which is defined as $\gamma_{\rm vM}(i) = \{E_{xy}(i)^2 + 1/2[E_{xx}(i) - E_{yy}(i)]\}^{1/2}$ for 2D systems [58]. Here, $E_{\alpha\beta}(i)$ is the $\alpha\beta$ component of the atomic Green-Lagrangian strain tensor E [59].

Our obtained distributions of the averaged shear strain for three different dislocation slip directions are presented in Fig. 3. For the dislocation slip direction $\theta \approx 0$ in Fig. 3(a), two channels with significant shear deformations exactly

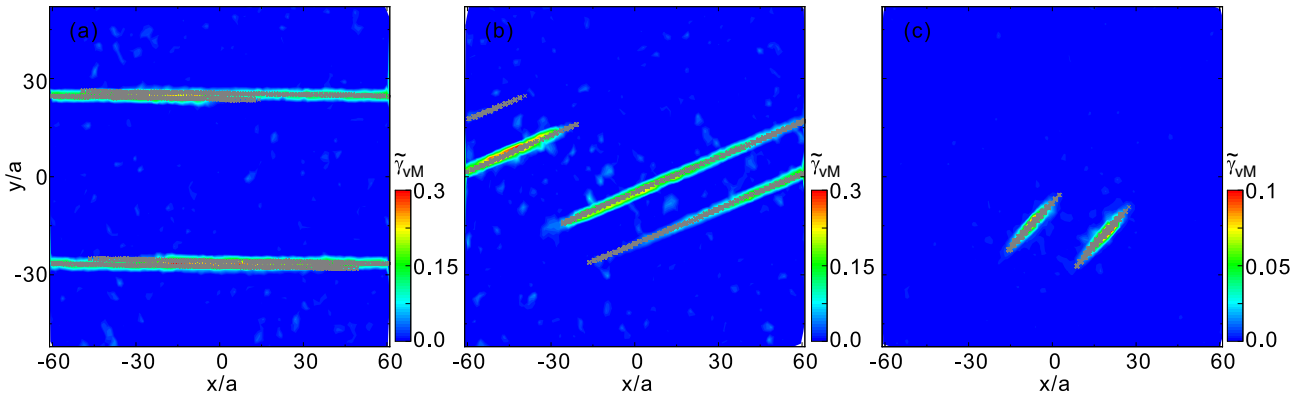

FIG. 3. Obtained distribution of the atomic shear strain $\widetilde{\gamma_{vM}(i)}$ in one shear deformation period for $\theta \approx 0$ (a), $\theta = \pi/9$ (b), and $\theta = \pi/4$ (c), respectively. All crosses correspond to various locations of two dislocations within one shear deformation period. When $\theta \approx 0$ in (a), the corresponding IF is the largest, where the trajectories of two dislocations result in two remarkable shear bands as they travel. However, when $\theta = \pi/4$ in (c), the corresponding IF is nearly zero, where the two dislocations do not move further, so that the shear strain is localized within limited regions around the two dislocations. For $\theta = \pi/9$ in (b), the strain evolution is somewhere between those for $\theta \approx 0$ and $\pi/4$.

follow the trajectories of the two dislocations, while the rest of the region is nearly undeformed. However, when $\theta = \pi/4$ in Fig. 3(c) for the nearly zero value of Q^{-1}, the two dislocations do not move much further during the shear deformation, so that the shear strain is only localized around the two dislocations. When $\theta = \pi/9$ in Fig. 3(b), the dislocation's slip distance is much more significant than that for $\theta = \pi/4$ and less than that for $\theta = 0$. These results clearly indicate that the mechanical energy dissipation is related to the two shear bands caused by the slip motion of two dislocations. The longer the slip distance, the greater the energy dissipation, i.e., the larger the IF.

Furthermore, we also calculate the distribution of the mean of the atomic elastic constant $\overline{C_{xyxy}(i)}$, as shown in Fig. 4. Following Eq. (3) of Ref. [47], we calculate the atomic elastic constant $C_{xyxy}(i)$ from the individual particle motion. We also obtain the mean of the calculated $C_{xyxy}(i)$ within one shear deformation period, marked as $\overline{C_{xyxy}(i)}$. As shown in the color bar of Fig. 4, the average of the mean of the atomic elastic constant $\overline{C_{xyxy}(i)}$ for all particles within the whole simulation region is marked as $\langle\overline{C_{xyxy}(i)}\rangle$. For the reported three dislocation slip angles in Fig. 4, our obtained $\langle\overline{C_{xyxy}(i)}\rangle$ value is always around $0.043\sigma_0$, well agreeing with the theoretical shear modulus value $0.040\sigma_0$ obtained from the transverse sound speed of the 2D Yukawa lattice [55]. For $\theta \approx 0$ in Fig. 4(a), the distribution of $\overline{C_{xyxy}(i)}$ in the entire simulation region is divided into two regions by the trajectories of the two dislocations, corresponding to the higher and lower elastic strengths, respectively. However, for $\theta = \pi/4$, as in Fig. 4(c), the $\overline{C_{xyxy}(i)}$ values for the particles around the dislocation trajectories increase significantly and are approximately 1.5 times larger than the $\langle\overline{C_{xyxy}(i)}\rangle$ values. Thus, when $\theta = \pi/4$, the local lattice around dislocations is able to sustain higher shear deformations, so that dislocations there do not move further, as observed in Fig. 3(c). When $\theta = \pi/9$ in Fig. 4(b), the distribution of $\overline{C_{xyxy}(i)}$ is similar to that for $\theta \approx 0$ in Fig. 4(a), also containing some features of $\theta = \pi/4$. Note that we also calculate the distributions of $\widetilde{\gamma_{vM}(i)}$ and $\overline{C_{xyxy}}$ for $\theta \approx \pi/2$,

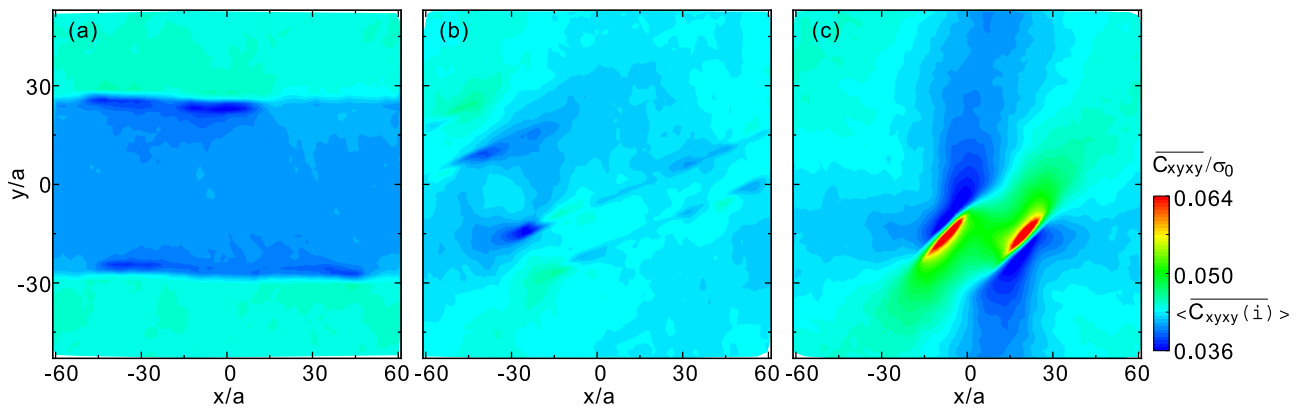

FIG. 4. Obtained distribution of the mean of the atomic elastic constant $\overline{C_{xyxy}}$ in one shear deformation period for $\theta \approx 0$ (a), $\theta = \pi/9$ (b), and $\theta = \pi/4$ (c), respectively. For $\theta \approx 0$ in (a), the whole simulation region is divided into two parts by the trajectories of two dislocations with two distinctive elastic constants. However, for $\theta = \pi/4$ in (c), the $\overline{C_{xyxy}}$ value of the local lattice around the dislocation trajectories increases significantly, indicating that this portion is able to sustain a higher rate of shear deformation. For $\theta = \pi/9$ in (b), the contour of the mean of the atomic elastic constant $\overline{C_{xyxy}}$ is mainly similar to that of $\theta = 0$ with some feathers of $\theta = \pi/4$.

which are almost the same as the results for $\theta \approx 0$ in Figs. 3(a) and 4(a) with just a 90° rotation, probably indicating the same IF mechanism for $\theta \approx 0$ and $\theta \approx \pi/2$ as also observed in Fig. 2.

Based on the results presented above, we provide our speculation about the observed dislocation IF. The generation of the dislocation IF is directly related to the slip distance of dislocations. When the value of Q^{-1} is not zero, due to the longer slip distance of dislocations, the particles on both sides of dislocations are totally rearranged, so that the shear bands through the crystal are generated. Due to the shear bands induced by the dislocations' slip motion, the elastic constant of the lattice on one side of the shear bands increases, while the elastic constant of the other side decreases. The decrease of the elastic constant results in the corresponding decrease of the stress, so that it is easier for dislocations to slip further, as shown in Fig. 4(a). However, when dislocations slip along $\theta = \pi/4$, even though the level of the shear stress amplitude is almost twice as high as $\theta \approx 0$, as shown in Figs. 1(b) and 1(c), it is still difficult for dislocations to slip further away, probably due to the anisotropy of our studied 2D solids. Our observed anisotropy of the dislocation motion above is similar to the feature reported in Ref. [60], where the mixed dislocations in the fcc metals have different mobilities under varied loading conditions, due to the phonon drag and radiative damping. We speculate that the resistance of the dislocation moving in various directions is also different, leading to different slip motion for dislocations. As a result, the round-trip motion of dislocations in the limited regions leads to a substantial increase of the elastic constant of the surrounding lattice, as shown in Fig. 4(c), further limiting the slide motion of dislocations, so that the IF nearly does not occur any more. Note that for systems at higher temperatures with more dislocations, the interaction between dislocations probably becomes substantial, combined with the severe thermal excitations, leading to a much more complicated IF mechanism, which is definitely different from the anelastic IF studied here, well beyond the scope of this paper.

C. Anelastic dislocation IF

As the secondary significant result of this paper, we find that the reported dislocation IF in 2D Yukawa solids exhibits a typical anelastic property.

As presented in Fig. 5(a), we find that the dislocation IF is nearly independent of the shear strain amplitude. In this investigation, the shear strain amplitude γ_0 varies from 0.019 to 0.057; however, the shear deformation frequency and the dislocation's slip angle are specified to be unchanged as $\omega/\omega_{pd} = 0.001$ and $\theta \approx 0$, respectively. From Fig. 5(a), as the shear strain amplitude increases from 0.019 to three times that value, the obtained Q^{-1} values are nearly unchanged around 0.53, only fluctuating very briefly. These obtained dislocation IF results clearly suggest that the dislocation IF is independent of the shear strain amplitude, satisfying one of the key characteristics of the anelastic property [11].

We also find that the dislocation IF is heavily dependent on the shear deformation frequency. The variation trend of the dislocation IF with the shear deformation frequency ω is presented in Fig. 5(b), under the conditions of the unchanged shear strain amplitude $\gamma_0 \approx 0.038$ and the constant dislocation slip angle $\theta \approx 0$. Within the shear deformation frequency range studied here, there is a prominent peak of Q^{-1} located at the frequency $\omega/\omega_{pd} \approx 0.001$. This prominent peak in Fig. 5(b) clearly indicates the strong dependence of the dislocation IF on the frequency ω. Thus our observed dislocation IF of 2D Yukawa solids possesses the two primary characteristics of anelasticity [11] simultaneously, clearly indicating that our observed dislocation IF is an anelastic behavior. These findings greatly deepen our fundamental understanding of the mechanical properties of 2D Yukawa solids, which may be experimentally verified in future.

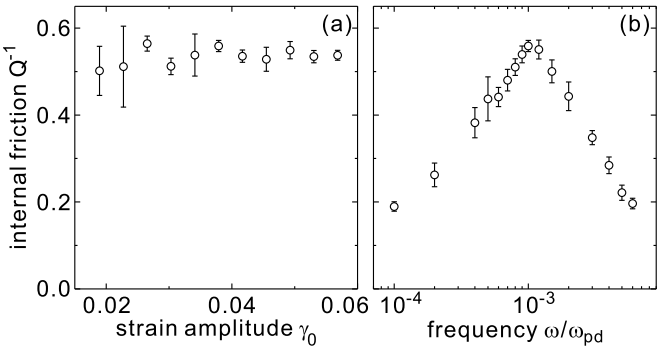

FIG. 5. Obtained variation of the dislocation IF Q^{-1} as functions of the shear strain amplitude γ_0 (a) and the shear deformation frequency ω (b). When the shear deformation frequency is specified as $\omega/\omega_{pd} = 0.001$ as in (a), the obtained IF values are almost unchanged under various shear strain amplitudes. When the shear strain amplitude is specified as $\gamma_0 \approx 0.038$ as in (b), there is a prominent peak of the IF centered at the shear deformation frequency $\omega/\omega_{pd} \approx 0.001$. Clearly, the observed dislocation IF mainly depends on the shear deformation frequency and is nearly independent of the shear strain amplitude, satisfying a typical anelastic property. Note that all data points shown here are obtained with a dislocation slip angle of $\theta \approx 0$.

IV. SUMMARY

In summary, we perform Langevin dynamics simulations to study the dislocation IF in solid 2D dusty plasmas with oscillating shear deformations. From the obtained stress-strain response, we determine the magnitude of dislocation IF for 2D Yukawa solids. We discover that the magnitude of dislocation IF is significantly dependent on the dislocation's slip direction relative to the shear direction. To investigate the underlying mechanism, we calculate the distributions of the atomic shear strain and elastic constant. We find that the variation trend of dislocation IF with the dislocation's slip direction is related to the slip distance of dislocations. The energy dissipation process may be accomplished by the formation of shear bands. Furthermore, we also find that the dislocation IF in 2D Yukawa solids is an anelastic behavior, since it is heavily dependent on the shear deformation frequency and nearly independent of the shear strain amplitude.

ACKNOWLEDGMENT

This work was supported by the National Natural Science Foundation of China under Grant No. 12175159,

the 1000 Youth Talents Plan, startup funds from Soochow University, and the Priority Academic Program Development (PAPD) of Jiangsu Higher Education Institutions.

[1] C. M. Zener, *Elasticity and Anelasticity of Metals* (University of Chicago Press, Chicago, 1948).
[2] R. de Batist, *Internal Friction of Structural Defects in Crystalline Solids* (North-Holland, Amsterdam, 1973).
[3] A. Puškár, *Internal Friction of Materials* (Cambridge International Science, Cambridge, 2001).
[4] M. S. Blanter, I. S. Golovin, H. Neuhäuser, and H. R. Sinning, *Internal Friction in Metallic Materials: A Handbook* (Springer-Verlag, Berlin, 2007).
[5] M. D. LaHaye, O. Buu, B. Camarota, and K. C. Schwab, Approaching the quantum limit of a nanomechanical resonator, Science **304**, 74 (2004).
[6] Y. Shi, P. Cui, Q. P. Kong, W. B. Jiang, and M. Winning, Internal friction peak in bicrystals with different misorientations, Phys. Rev. B **71**, 060101(R) (2005).
[7] J. Wu and C. C. Yu, How stress can reduce dissipation in glasses, Phys. Rev. B **84**, 174109 (2011).
[8] H. Wagner, D. Bedorf, S. Kuchemann, M. Schwabe, B. Zhang, W. Arnold, and K. Samwer, Local elastic properties of a metallic glass, Nat. Mater. **10**, 439 (2011).
[9] H. Yu and K. Samwer, Atomic mechanism of internal friction in a model metallic glass, Phys. Rev. B **90**, 144201 (2014).
[10] L. Wang, Q. Zhang, Z. Huang, X. Cui, and F. Zu, Study of the mechanism of the internal friction peak in a $Cu_{36}Zr_{48}Al_8Ag_8$ bulk metallic glass, J. Non-Cryst. Solids **406**, 127 (2014).
[11] A. S. Nowick and B. S. Berry, *Anelastic Relaxation in Crystalline Solids* (Academic, New York, 1972).
[12] H. M. Thomas and G. E. Morfill, Melting dynamics of a plasma crystal, Nature (London) **379**, 806 (1996).
[13] L. I, W. Juan, C. Chiang, and J. Chu, Microscopic particle motions in strongly coupled dusty plasmas, Science **272**, 1626 (1996).
[14] A. Melzer, A. Homann, and A. Piel, Experimental investigation of the melting transition of the plasma crystal, Phys. Rev. E **53**, 2757 (1996).
[15] M. S. Murillo, Critical wave vectors for transverse modes in strongly coupled dusty plasmas, Phys. Rev. Lett. **85**, 2514 (2000).
[16] R. L. Merlino and J. A. Goree, Dusty plasmas in the laboratory, industry, and space, Phys. Today **57**(7), 32 (2004).
[17] G. J. Kalman, P. Hartmann, Z. Donkó, and M. Rosenberg, Two-dimensional Yukawa liquids: Correlation and dynamics, Phys. Rev. Lett. **92**, 065001 (2004).
[18] V. E. Fortov, A. V. Ivlev, S. A. Khrapak, A. G. Khrapak, and G. E. Morfill, Complex (dusty) plasmas: Current status, open issues, perspectives, Phys. Rep. **421**, 1 (2005).
[19] G. E. Morfill and A. V. Ivlev, Complex plasmas: An interdisciplinary research field, Rev. Mod. Phys. **81**, 1353 (2009).
[20] A. Piel, *Plasma Physics* (Springer, Heidelberg, 2010).
[21] M. Bonitz, C. Henning, and D. Block, Complex plasmas: A laboratory for strong correlations, Rep. Prog. Phys. **73**, 066501 (2010).
[22] A. Melzer, A. Schella, J. Schablinski, D. Block, and A. Piel, Analyzing the liquid state of two-dimensional dust clusters: The instantaneous normal mode approach, Phys. Rev. E **87**, 033107 (2013).
[23] E. Thomas, Jr., U. Konopka, R. L. Merlino, and M. Rosenberg, Initial measurements of two-and three-dimensional ordering, waves, and plasma filamentation in the magnetized dusty plasma experiment, Phys. Plasmas **23**, 055701 (2016).
[24] S. Jaiswal, T. Hall, S. LeBlanc, R. Mukherjee, and E. Thomas, Effect of magnetic field on the phase transition in a dusty plasma, Phys. Plasmas **24**, 113703 (2017).
[25] W. Yu, J. Cho, and J. C. Burton, Extracting forces from noisy dynamics in dusty plasmas, Phys. Rev. E **106**, 035303 (2022).
[26] Y. Feng, J. Goree, and B. Liu, Solid superheating observed in two-dimensional strongly coupled dusty plasma, Phys. Rev. Lett. **100**, 205007 (2008).
[27] K. Qiao, J. Kong, J. Carmona-Reyes, L. S. Matthews, and T. W. Hyde, Mode coupling and resonance instabilities in quasi-two-dimensional dust clusters in complex plasmas, Phys. Rev. E **90**, 033109 (2014).
[28] L. Couëdel and V. Nosenko, Stability of two-dimensional complex plasma monolayers in asymmetric capacitively coupled radio-frequency discharges, Phys. Rev. E **105**, 015210 (2022).
[29] Z. Donkó, J. Goree, P. Hartmann, and K. Kutasi, Shear viscosity and shear thinning in two-dimensional Yukawa liquids, Phys. Rev. Lett. **96**, 145003 (2006).
[30] C. Chan and Lin I, Viscoelastic response of mesoscopic dusty-plasma liquids, Phys. Rev. Lett. **98**, 105002 (2007).
[31] B. Liu and J. Goree, Superdiffusion and non-Gaussian statistics in a driven-dissipative 2D dusty plasma, Phys. Rev. Lett. **100**, 055003 (2008).
[32] T. Ott and M. Bonitz, Is diffusion anomalous in two-dimensional Yukawa liquids, Phys. Rev. Lett. **103**, 195001 (2009).
[33] Y. Feng, J. Goree, and B. Liu, Viscoelasticity of 2D liquids quantified in a dusty plasma experiment, Phys. Rev. Lett. **105**, 025002 (2010).
[34] M. S. Murillo, Strongly coupled plasma physics and high energy-density matter, Phys. Plasmas **11**, 2964 (2004).
[35] A. Melzer, A. Schella, J. Schablinski, D. Block, and A. Pie, Instantaneous normal mode analysis of melting of finite dust clusters, Phys. Rev. Lett. **108**, 225001 (2012).
[36] P. Hartmann, A. Douglass, J. C. Reyes, L. S. Matthews, T. W. Hyde, A. Kovács, and Z. Donkó, Crystallization dynamics of a single layer complex plasma, Phys. Rev. Lett. **105**, 115004 (2010).
[37] E. Thomas, Jr., B. Lynch, U. Konopka, R. L. Merlino, and M. Rosenberg, Observations of imposed ordered structures in a dusty plasma at high magnetic field, Phys. Plasmas **22**, 030701 (2015).
[38] C. Durniak and D. Samsonov, Plastic deformations in complex plasmas, Phys. Rev. Lett. **106**, 175001 (2011).
[39] P. Hartmann, A. Z. Kovács, A. M. Douglass, J. C. Reyes, L. S. Matthews, and T. W. Hyde, Slow plastic creep of 2D dusty plasma solids, Phys. Rev. Lett. **113**, 025002 (2014).

[40] J. D. Williams, E. Thomas, L. Couëdel, A. V. Ivlev, S. K. Zhdanov, V. Nosenko, H. M. Thomas, and G. E. Morfill, Kinetics of the melting front in two-dimensional plasma crystals: Complementary analysis with the particle image and particle tracking velocimetries, Phys. Rev. E **86**, 046401 (2012).

[41] A. Piel, V. Nosenko, and J. Goree, Experiments and molecular-dynamics simulation of elastic waves in a plasma crystal radiated from a small dipole source, Phys. Rev. Lett. **89**, 085004 (2002).

[42] B. Liu and J. Goree, Determination of yield stress of 2D (Yukawa) dusty plasma, Phys. Plasmas **24**, 103702 (2017).

[43] W. Li, W. Lin, and Y. Feng, Bulk modulus of two-dimensional liquid dusty plasmas and its application, Phys. Plasmas **24**, 043702 (2017).

[44] Y. Feng, D. Huang, and W. Li, Adiabatic bulk modulus of elasticity for 2D liquid dusty plasmas, Phys. Plasmas **25**, 057301 (2018).

[45] S. Khrapak and B. Klumov, High-frequency elastic moduli of two-dimensional Yukawa fluids and solids, Phys. Plasmas **25**, 033706 (2018).

[46] K. Wang, D. Huang, and Y. Feng, Shear modulus of two-dimensional Yukawa or dusty-plasma solids obtained from the viscoelasticity in the liquid state, Phys. Rev. E **99**, 063206 (2019).

[47] S. Lu, D. Huang, and Y. Feng, Shear softening and hardening of a two-dimensional Yukawa solid, Phys. Rev. E **105**, 035203 (2022).

[48] Z. Donkó, J. Goree, P. Hartmann, and K. Kutasi, Viscoelastic response of Yukawa liquids, Phys. Rev. E **81**, 056404 (2010).

[49] S. Lu, D. Huang, and Y. Feng, Plastic strain rate quantified from dislocation dynamics in dusty plasma shear flows, Phys. Rev. E **103**, 063214 (2021).

[50] S. Plimpton, Fast parallel algorithms for short-range molecular-dynamics, J. Comput. Phys. **117**, 1 (1995); https://www.lammps.org/#gsc.tab=0.

[51] B. A. Klumov and G. E. Morfill, Structural properties of complex (dusty) plasma upon crystallization and melting, JETP Lett. **90**, 444 (2009).

[52] Y. Feng, B. Liu, and J. Goree, Rapid heating and cooling in two-dimensional Yukawa systems, Phys. Rev. E **78**, 026415 (2008).

[53] P. Hartmann, G. J. Kalman, Z. Donkó, and K. Kutasi, Equilibrium properties and phase diagram of two-dimensional Yukawa systems, Phys. Rev. E **72**, 026409 (2005).

[54] M. P. Allen and D. J. Tildesley, *Computer Simulation of Liquids* (Clarendon, Oxford, 1987).

[55] X. Wang, A. Bhattacharjee, and S. Hu, Longitudinal and transverse waves in Yukawa crystals, Phys. Rev. Lett. **86**, 2569 (2001)

[56] N. A. Tyapunina, E. K. Naimi, and S. V. Gasparyan, The orientation dependence of dislocation internal friction in real crystals. I. Alkali halide crystals, Phys. Status Solidi A **46**, 351 (1978).

[57] N. A. Tyapunina, E. K. Naimi, S. V. Gasparyan, and G. M. Zinenkov, The orientation dependence of dislocation internal friction in real crystals. II. Hexagonal crystals, Phys. Status Solidi A **46**, 411 (1978).

[58] F. Shimizu, S. Ogata, and J. Li, Theory of shear banding in metallic glasses and molecular dynamics calculations, Mater. Trans. **48**, 2923 (2007).

[59] J. Lubliner, *Plasticity Theory* (Dover, Berkeley, CA, 2006).

[60] N. Burbery, R. Das, and W. G. Ferguson, Dynamic behaviour of mixed dislocations in FCC metals under multi-oriented loading with molecular dynamics simulations, Comput. Mater. Sci. **137**, 39 (2017).